geosciences

MDPI

Article

Recent Trends and Regime Shifts in Arctic Coastal Temperatures: Evidence of AMOC Slowing?

Elena A. Kasatkina *, Oleg I. Shumilov and Dmitry V. Makarov

Institute of North Industrial Ecology Problems, Kola Science Center, Russian Academy of Sciences, 184209 Apatity, Russia; o.shumilov@ksc.ru (O.I.S.); d.makarov@ksc.ru (D.V.M.)
* Correspondence: e.kasatki@yandex.ru; Tel.: +7-(81555)-78620

Abstract

This study analyzes surface air temperature (SAT) trends at 158 stations located on or above the Arctic Circle over the 2000–2024 period, aiming to assess whether recent temperature shifts could serve as indirect indicators of a slowing Atlantic Meridional Overturning Circulation (AMOC). Regression analysis reveals that only 40% of stations show statistically significant warming trends ($p < 0.05$), while 33% exhibit no significant trend. Applying the Pettitt and Buishand tests, we detect abrupt regime shifts at 38 stations, with breakpoints concentrated between 2009 and 2014. Notably, 36 of these stations display a weakening of the warming trend after the breakpoint: at 13 stations (including key Arctic archipelagos and the White Sea coast), an initial increase shifts to a decrease; at 17 stations, warming continues but at a slower rate; and at 6 stations (near the Bering Strait), a decrease intensifies. These spatial patterns suggest a potential fingerprint of AMOC slowdown, consistent with recent modeling studies that predict cooling in northwestern Europe and possible Little Ice Age-type environmental conditions. Our findings have implications for assessing future Arctic navigation, coastal infrastructure, and resource extraction under changing climate regimes.

Keywords: temperature trends; ocean current system; Arctic

1. Introduction

The global economy's rising susceptibility to climate-related impacts has recently intensified attention on climate change. According to the Sixth Assessment Report of the Intergovernmental Panel on Climate Change (IPCC), continued global warming will intensify environmental and socio-economic risks [1]. Coastal areas and islands are particularly vulnerable, as climate change and associated sea level rise may lead to catastrophic environmental changes and population displacement [1]. However, for northern high-latitude regions, climate change presents both risks and opportunities. Increased river runoff and melting of sea ice heighten environmental risks, but at the same time, they create opportunities for Arctic navigation and natural resource extraction [2,3]. These resources could be mined far more intensively if trade routes and related infrastructure along the Northern Sea Route were sufficiently developed. The Russian Arctic holds rich deposits of gas, oil, copper-nickel ores, fertilizer ores, platinum-group metals, rare and rare earth elements, gold diamonds, ferrous metals and other mineral resources [4,5]. Declining sea ice extent will generate new trade opportunities, particularly along the Northern Sea Route, which runs along Russia's coastline [3,6]. Moreover, global logistics restructuring—driven by geopolitical instability in the Middle East—has created additional opportunities for

Check for updates

Academic Editors: Christian Natale Gencarelli and Enrique Sanchez

Received: 5 May 2026
Revised: 16 June 2026
Accepted: 17 June 2026
Published: 19 June 2026

Copyright: © 2026 by the authors. Licensee MDPI, Basel, Switzerland. This article is an open access article distributed under the terms and conditions of the Creative Commons Attribution (CC BY) license.

the development of Arctic sea routes [7,8]. These routes offer a shortcut between Atlantic and Pacific ports, reducing distances by 30% to 60% compared to the Suez and Panama Canal routes [7].

Recent studies have shown that climatic changes in the Arctic are consistent with fluctuations in the intensity of the Atlantic Meridional Overturning Circulation (AMOC) [9–12]. The AMOC is a key component of the Earth's ocean circulation system, transporting up to 25% of the total northward heat from the Southern Hemisphere to the Northern Hemisphere [9]. Results from recent simulations indicate that an AMOC collapse would cool Europe by several degrees [11,12]. However, the causes of the AMOC weakening remain debated. Most often, AMOC changes are linked to global warming and the associated freshening of the North Atlantic due to increased river runoff, sea ice melting, and glacier retreat [1,13]. Other researchers attribute the future slowdown of the AMOC to Sun–Earth interactions [14] and variations in solar activity [15]. According to this line of evidence, the circulation pattern in the North Atlantic changed dramatically during Grand Solar Minima [14,15]. For instance, Mörner proposed that changes in the Earth's rotation alter the North Atlantic circulation system during such minima of solar activity [14]. Based on these findings, similar conditions are likely to recur during the approaching Grand Solar Minimum (GSM) in the 21st century [14]. During such a period of low solar activity—the Maunder Minimum (1645–1715 AD)—total solar irradiance (TSI) decreased by about 3 W/m^2 [16]. This reduction was associated with a 1.5 °C drop in Northern Hemisphere temperatures [17]. The period coincided with harsher winters and the freezing of rivers across Europe [17]. Other studies provide evidence for an approaching GSM, which, according to these authors, could bring Little Ice Age-like climatic conditions in the 21st century [18–21].

To assess whether a slowdown or even collapse of the AMOC is likely in the near future, we evaluate climatic changes in Arctic coastal regions. For this purpose, we analyze surface air temperature (SAT) trends at sites located on or above the Arctic Circle over the period from 2000 to 2024. The results will also help determine whether shifts in surface air temperature in coastal regions might provide indirect evidence consistent with AMOC variability.

2. Materials and Methods

2.1. Data

Annual SAT data from meteorological stations in the GISTEMP database [22] were used to assess recent temperature trends in the Arctic. In total, data of 158 stations located on the Arctic coastal region, and either near or above the Arctic Circle, were used. These stations spread across eight countries: Russia, the USA, Canada, Denmark (Greenland), Norway, Sweden, Finland, and Iceland (Figure 1 and Table S1).

2.2. Trend Test

To analyze the temporal temperature trends at 158 Arctic stations, we employed a combination of parametric and nonparametric methods. Ordinary least squares regression (OLS) and segmented (piecewise) regression were used to model linear and potential change-point trends. For robust trend detection without distributional assumptions, we applied the Mann–Kendall test, Sen's slope estimator, Pettitt's change-point test, and the Buishand test with a permutation approach [23–27].

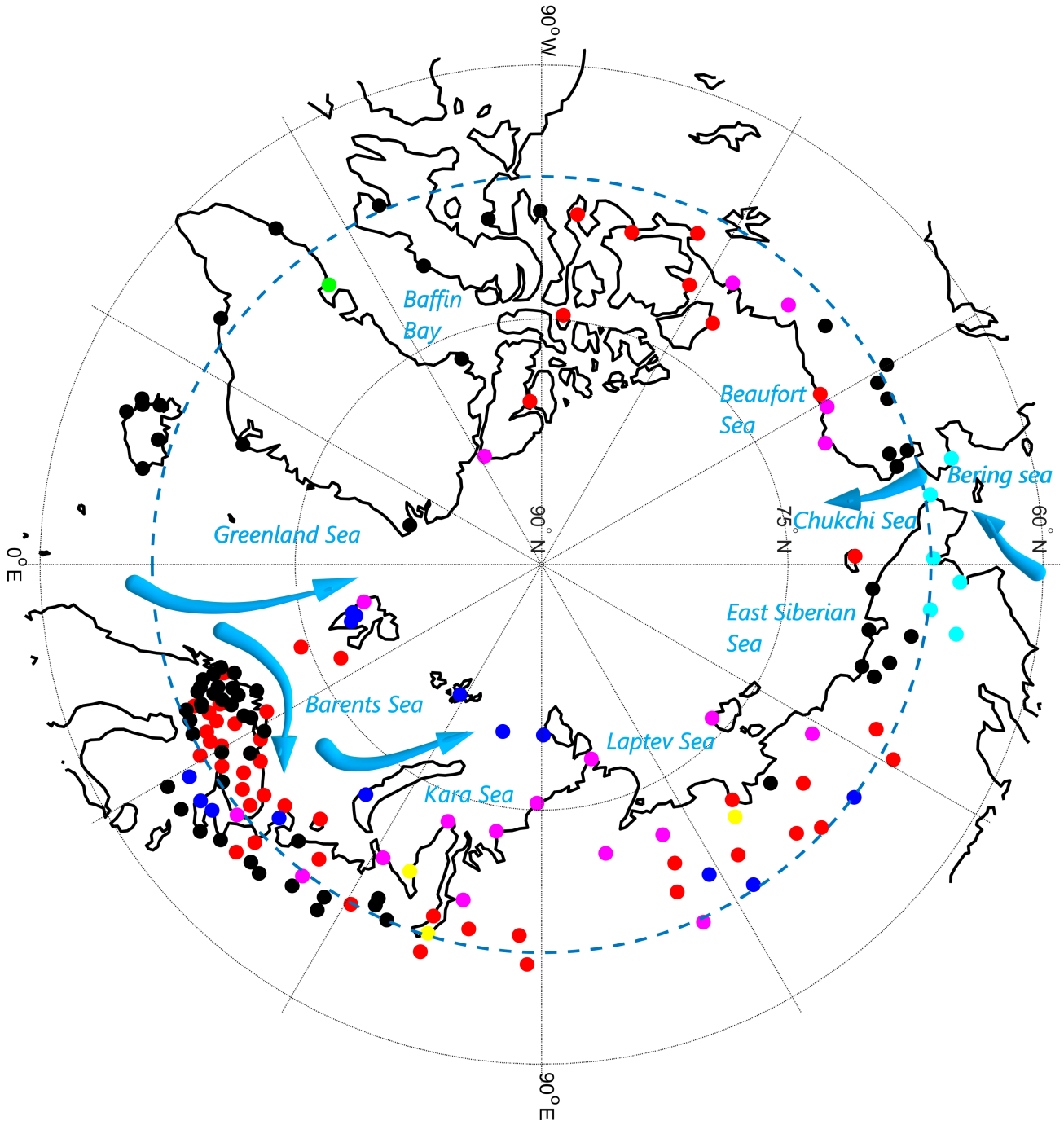

Figure 1. Locations of the 158 stations used in this study. Stations with a downward temperature shift are marked as follows: blue circles for an increase followed by a decrease, cyan circles for a decrease followed by a stronger decrease, and magenta circles for an increase followed by a weaker increase. Stations with an upward shift are shown as purple circles. Three stations with a temperature increase followed by a stronger increase are marked by yellow circles. Stations exhibiting a significant increasing trend are indicated by red circles, while those with no significant trend are shown as black circles. One station exhibiting a significant decreasing trend is indicated by green circle. Blue arrows show the inflows of Atlantic and Pacific waters. Arctic Circle is shown by a dushed blue line.

2.2.1. Ordinary Linear Regression

For each station, the temperature time series X_t ($t = 1, \ldots, N$) was modelled as

$$X_t = a + b + t + \varepsilon_t \quad (1)$$

where a is the intercept, b the trend coefficient (estimated by ordinary least squares), and ε_t the residuals. The significance of b was assessed using the t-test.

2.2.2. Segmented Regression (Two-Phase Linear Model)

To allow for a single abrupt change in trend, we fitted a two-segment model:

$$X_t = \begin{cases} a_1 + b_1 \cdot t + \varepsilon_t, & t \le \tau, \\ a_2 + b_2 \cdot t + \varepsilon_t & t > \tau, \end{cases} \quad (2)$$

where τ is the breakpoint (year). The parameters a_1, b_1, a_2, and b_2 were estimated by least squares.

2.2.3. Mann–Kendall Trend Test

The Mann–Kendall test is a nonparametric approach based on data ranking, used to identify trends in time series without assuming linearity or normality. It has been extensively used to evaluate trends in hydro-meteorological time series [23,24]. The null hypothesis of no monotonic trend was tested using the Kendall's S statistic [23]:

$$S = \sum_{i=1}^{N-1} \sum_{j=i+1}^{N} sgn(X_j - X_i), \quad (3)$$

with $sgn(x)$ = 1, 0, −1 for x > 0, =0, <0 respectively. For $n \ge 10$, the variance of S is

$$Var(S) = \frac{n(n-1)(2n+5) - \sum_k t_k(t_k-1)(2t_k+5)}{18}, \quad (4)$$

where t_k are the sizes of tied groups. The standardized test statistic Z is

$$Z = \begin{cases} \frac{S-1}{\sqrt{Var(S)}}, & S > 0, \\ 0, & S = 0, \\ \frac{S+1}{\sqrt{Var(S)}}, & S < 0. \end{cases} \quad (5)$$

2.2.4. Sen's Slope Estimator

The Sen's slope estimator is a reliable nonparametric method to estimate slope, serving as a viable alternative to the least-squares method [25]. The magnitude of the monotonic trend was estimated by Sen's slope, the median of all pairwise slopes:

$$\beta = median\left(\frac{X_j - X_i}{j - i}\right), \ \forall i < j \quad (6)$$

2.2.5. Pettitt's Change-Point Test

In this study, we used the nonparametric Pettitt test for breakpoint (change point) analysis [26]. The Pettitt test is a rank-based procedure that detects a shift in the mean at an unknown time point and assesses its statistical significance. The test employs a version of the Mann–Whitney statistic $U_{t,N}$, which evaluates whether two samples $X_1, \ldots, X_t$ and $X_{t+1}, \ldots, X_N$ originate from the same population. The null hypothesis H_0 states that no breakpoint exists, whereas the alternative hypothesis H_1 assumes that a breakpoint occurs at some unknown time. The test statistic is defined as [26]

$$U_{t,N} = \sum_{i=1}^{t} \sum_{j=t+1}^{N} sgn\ (X_i - X_j), \quad (7)$$

The most significant breakpoint is identified as the time t that maximizes the absolute value of $U_{t,N}$:

$$K_N = max_{1 \le t < N} |U_{t,N}| \quad (8)$$

A key advantage of the Pettitt test is its robustness to outliers and skewed distributions compared to parametric alternatives. Moreover, an approximate p-value can be computed as [26]

$$p = 2exp\left(\frac{-6K_N^2}{N^3 + N^2}\right) \quad (9)$$

If the resulting p-value is less than a pre-specified significance level α (here, $\alpha = 0.05$), the null hypothesis is rejected, and the time series is split into two segments at the estimated breakpoint location t.

2.2.6. Buishand Test with Permutation

In addition to the Pettitt test, the Buishand test with a permutation approach [27] was used to assess the change-point in temperature trends. The Buishand test is based on the adjusted partial sums [27]:

$$S_k = \sum_{i=1}^{k} (X_i - \overline{X}), k = 1, \ldots, N, \quad (10)$$

with $\overline{X}$ the overall mean. The test statistic Q is

$$Q = \frac{\max\limits_{1 \le k \le N} |S_k|}{\sigma} \quad (11)$$

where σ is the sample standard deviation.

When applying with permutation (i.e., using a permutation procedure to estimate the null distribution of the test statistics), the Buishand test becomes essentially nonparametric [27]. The original Buishand test often assumes normality for the data distribution. With permutation, we avoid this assumption entirely. The test statistic is computed on the original data, and then the data are repeatedly shuffled (permuted). Under the null hypothesis (no change point), all permutations are equally likely. To obtain a robust p-value without assuming normality, we used a permutation approach: the time series was randomly reordered 10,000 times, and Q recomputed for each permutation. The p-value was the fraction of permuted statistics exceeding the observed Q.

All statistical analyses were carried out with GNU Octave (version 11.1.0).

3. Results

Temperature trends at 158 Arctic stations over the period 2000–2024 were estimated using ordinary least-squares (OLS) regression, the Mann–Kendall (MK) test and Sen's slope estimator (SSE). Trend magnitudes obtained from parametric and nonparametric approaches were highly consistent, with a Spearman correlation coefficient of $r = 0.895$ ($p < 0.001$) between the two arrays of trend estimates. Given this strong agreement, only the Mann–Kendall and Sen's slope results are presented in Table S1.

The combination of the MK test and SSE revealed that only 49 stations (31%) exhibited statistically significant increasing trends ($p < 0.05$), with Sen's slopes ranging from 0.032 to 0.118 °C per year (Figure 1 and Table S1). A further 66 stations (42%) showed no statistically significant trend ($p \ge 0.05$; Table S1). These 66 stations were predominantly located in the USA, Greenland, Iceland, mainland Norway and Sweden (Figure 1 and Table S1). In contrast, nearly all stations in the Canadian Arctic Archipelago and Murmansk Oblast

(Russia) showed significant increasing trends over the same period. In Finland, stations were approximately equally divided between those with positive trends and those with no significant trends.

The homogeneity of the annual mean SAT time series was tested using two nonparametric methods: the Pettitt test and the permutation-based Buishand test. After identifying change points, each full time series (2000–2024) was divided into two segments: before and after the breakpoint. Linear trends for each segment were then estimated using segmented regression analysis (Equation (2)). The main statistical results are summarized in Table 1.

Table 1. Statistically significant regime shifts in annual mean Arctic surface air temperatures (2000–2024): breakpoints, trends and associated statistics.

Stations	Coordinates	Trend (°C/year) [2]	R^2	Pettitt Test		Buishand Test	
				BP (Year) [1]	p	BP (Year) [1]	p
Russia							
Pjalica	66.18 N, 39.53 E	+0.173; +0.027	0.56	2006 ↑↑	0.017	2011 ↑↑	0.024
Kalevala	65.20 N, 31.17 E	+0.006; −0.006	0.33	2013 ↑↓	0.037	2013 ↑↓	0.043
Kem	64.98 N, 34.82 E	+0.019; −0.015	0.43	2013 ↑↓	0.008	2013 ↑↓	0.006
Heiss Island	80.60 N, 58.00 E	+0.118; −0.078	0.46	2010 ↑↓	0.004	2010 ↑↓	0.005
M. Karmakuly	72.60 N, 38.00 E	+0.11; −0.005	0.37	2010 ↑↓	0.023	2010 ↑↓	0.042
Amderma	69.75 N, 61.70 E	+0.123; +0.007	0.41	2010 ↑↑	0.032	2010 ↑↑	0.048
Sojna	67.90 N, 44.10 E	+0.068; −0.015	0.40	2014 ↑↓	0.037	2014 ↑↓	0.12 **
Zhizhgin Mayak	65.20 N, 36.82 E	+0.013; −0.017	0.44	2013 ↑↓	0.009	2013 ↑↓	0.004
Okunev Nos	66.25 N, 52.58 E	+0.115; +0.022	0.42	2014 ↑↑	0.026	2010 ↑↑	0.03
Bely Island	73.33 N, 70.03 E	+0.11; +0.064	0.45	2010 ↑↑	0.014	2010 ↑↑	0.024
Marre Sale	69.72 N, 66.82 E	+0.102; +0.124	0.37	2010 ↑↑*	0.043	2010 ↑↑*	0.023
Antipajuta	69.08 N, 76.90 E	+0.155; +0.034	0.36	2010 ↑↑	0.046	2010 ↑↑	0.09 **
Nyda	66.63 N, 72.92 E	+0.009; +0.068	0.34	2010 ↑↑*	0.026	2010 ↑↑*	0.09 **
Golomyanny Island	79.55 N, 90.62 E	+0.221; −0.035	0.60	2009 ↑↓	0.002	2013 ↑↓	<0.001
Vize Island	79.50 N, 76.98 E	+0.257; −0.052	0.50	2009 ↑↓	0.002	2009 ↑↓	<0.001
GMO Im. Fedorova	77.72 N, 104.30 E	+0.009; +0.068	0.61	2009 ↑↑	0.001	2009 ↑↑	<0.001
Sterlegova	75.42 N, 88.90 E	+0.257; +0.025	0.51	2010 ↑↑	0.014	2010 ↑↑	0.015
Dikson	73.50 N, 80.40 E	+0.155; +0.007	0.41	2010 ↑↑	0.012	2010 ↑↑	0.035
Hatanga	71.98 N, 102.47 E	+0.156; +0.11	0.53	2010 ↑↑	0.007	2010 ↑↑	0.006
Kotelny Island	76.00 N, 137.87 E	+0.200; +0.055	0.67	2009 ↑↑	0.003	2009 ↑↑	0.003
Saskylah	71.97 N, 114.08 E	+0.201; +0.162	0.63	2009 ↑↑	0.003	2009 ↑↑	0.003
Kjusjur	70.68 N, 127.40 E	+0.055; +0.155	0.53	2014 ↑↑*	0.007	2010 ↑↑*	0.009
Chocurdah	70.62 N, 147.88 E	+0.084; +0.015	0.51	2013 ↑↑	0.008	2010 ↑↑	0.016
Suhana	68.62 N, 118.33 E	+0.096; −0.017	0.51	2013 ↑↓	0.005	2013 ↑↓	0.007
Zhigansk	66.77 N, 123.40 E	+0.096; −0.023	0.50	2013 ↑↓	0.008	2009 ↑↓	0.012
Ust Moma	66.45 N, 143.23 E	+0.079; −0.064	0.49	2013 ↑↓	0.009	2006 ↑↓	0.023
Selagoncy	66.25 N, 114.28 E	+0.115; +0.089	0.57	2010 ↑↑	0.006	2013 ↑↑	0.003
Enmuveem	66.38 N, 173.33 E	−0.054; −0.175	0.56	2013 ↓↓	0.025	2013 ↓↓	0.007
Egvekinot	66.35 N, 179.10 W	−0.044; −0.175	0.42	2013 ↓↓	0.037	2013 ↓↓	0.017
Mys Uelen	66.17 N, 169.80 W	−0.007; −0.173	0.47	2013 ↓↓	0.014	2013 ↓↓	0.006
Anadyr	64.78 N, 177.57 E	−0.016; −0.199	0.51	2013 ↓↓	0.020	2013 ↓↓	0.012
Markovo	64.68 N, 170.42 E	−0.062; −0.141	0.49	2013 ↓↓	0.020	2013 ↓↓	0.036
USA (AK)							
Barrow	71.28 N, 156.78 W	+0.102; +0.005	0.55	2013 ↑↑	0.004	2013 ↑↑	0.003
Nuiqsut	71.21 N, 151.00 W	+0.102; +0.005	0.50	2013 ↑↑	0.005	2013 ↑↑	0.008
Nome Muni	64.51 N, 165.44 W	−0.111; −0.222	0.58	2013 ↓↓	0.02	2013 ↓↓	0.014
Canada							
Alert (NU)	82.50 N, 62.33 W	+0.194; +0.059	0.60	2009 ↑↑	0.01	2009 ↑↑	0.011
Paulatuk (NT)	69.35 N, 124.08 W	+0.058; +0.052	0.36	2009 ↑↑	0.03	2009 ↑↑	0.069 **
Inuvik (NT)	68.30 N, 133.48 W	+0.088; +0.009	0.48	2009 ↑↑	0.008	2009 ↑↑	0.008

Table 1. *Cont.*

Stations	Coordinates	Trend (°C/year) [2]	R^2	Pettitt Test		Buishand Test	
				BP (Year) [1]	p	BP (Year) [1]	p
Norway (Svalbard)							
Ny Alesund	78.92 N, 11.93 E	+0.075; +0.023	0.49	2011 ↑↑	0.008	2013 ↑↑	0.010
Svalbard Airport	78.25 N, 15.47 E	+0.095; −0.029	0.44	2011 ↑↓	0.012	2013 ↑↓	0.030
Barentsburg	78.10 N, 14.30 E	+0.091; −0.016	0.50	2011 ↑↓	0.008	2011 ↑↓	0.009
Sveagruva	77.88 N, 16.72 E	+0.088; −0.071	0.46	2011 ↑↓	0.009	2011 ↑↓	0.008

[1] ↑↓ = increase followed by decrease; ↑↑ = increase followed by weaker increase; ↑↑* = increase followed by stronger increase; ↓↓ = decrease followed by stronger decrease. ** Stations where the Buishand test did not detect a breakpoint. [2] Trend before and after breakpoint (°C). See Figure 1 and Table S1 for geographical locations.

The Pettitt test detected breakpoints at strong ($p < 0.05$) or very strong ($p < 0.01$) significance levels at 42 of the 158 stations (27%). Among these, only three stations exhibited a strengthening of the positive temperature trend after the breakpoint (i.e., an increase followed by a steeper increase): Marre Sale, Nyda, and Kjusjur. The first two are located on opposite sides of the Yamal Peninsula, in coastal areas of the Kara Sea bays—the Gulf of Ob and Baydaratskaya Bay. The third station, Kjusjur (Sakha Republic, Yakutia), lies adjacent to the coastal zone of the Laptev Sea (Figure 1 and Table S1).

The Buishand test identified breakpoints at 38 stations (Table 1). Compared with the Pettitt results, the Buishand test confirmed breakpoints at 38 of the 42 stations identified by the Pettitt test. The four stations where the Buishand test did not detect a breakpoint were Sojna (Arkhangelsk Oblast, Russia), Antipajuta (Yamalo-Nenets Okrug, Russia), Nyda (Yamalo-Nenets Okrug, Russia), and Paulatuk (Canada). Thus, 38 stations showed breakpoints according to both tests. Excluding these four stations would not alter the main conclusions. Moreover, several studies based on real data suggest that the Pettitt test is more reliable for detecting inhomogeneities [28]. The timing of breakpoints was generally consistent between the two tests (Table 1). Only five stations deviated from this pattern: Pjalica (Murmansk Oblast, Russia), where the Pettitt test placed the breakpoint in 2006 ($p = 0.017$) and the Buishand test in 2011 ($p = 0.024$); Okunev Nos (Komi Republic, Russia), with breakpoints in 2014 (Pettitt, $p = 0.026$) and 2010 (Buishand, $p = 0.03$); Zhigansk (Sakha Republic, Russia), with breakpoints in 2013 (Pettitt, $p = 0.008$) and 2009 (Buishand, $p = 0.012$); Ust Moma (Sakha Republic, Russia), with breakpoints in 2013 (Pettitt, $p = 0.009$) and 2006 (Buishand, $p = 0.023$); and Selagoncy (Sakha Republic, Russia), with breakpoints in 2010 (Pettitt, $p = 0.006$) and 2013 (Buishand, $p = 0.003$). Nevertheless, even for these five stations, at least one of the two tests placed the breakpoint within the 2009–2014 interval (Table 1). The overall agreement between the two tests supports the robustness of the detected change points. Considering the agreement between two independent homogeneity tests and the broad spatial coverage (stations distributed across the entire Arctic north of 60° N), we conclude that the detected breakpoints are not artefacts of data inhomogeneity. Instead, they reflect real, physically driven external forcing that occurred around 2009–2014.

Of the 38 stations with breakpoints identified by both tests, two (Marre Sale and Kjusjur) showed a steeper increase after the breakpoint, as described above. Among the remaining 36 stations with the breakpoints, 13 (34%) showed an initial increase in mean annual SAT followed by a decrease after the breakpoint (Table 1). Examples of this pattern are shown in Figure 2: Svalbard Airport (Svalbard, Norway; Figure 2a), Heiss Island (Franz Josef Land, Russia; Figure 2b), and Zhizhgin Mayak (Arkhangelsk Oblast, Russia; Figure 2c). Six stations (16%) exhibited a decrease followed by a stronger decrease, as illustrated by Anadyr (Chukotka, Russia) in Figure 2d. Seventeen stations (45% of the 38) displayed an increase followed by a weaker increase, exemplified by Barrow (Alaska, USA; Figure 3a) and Alert (Canada, Figure 3b).

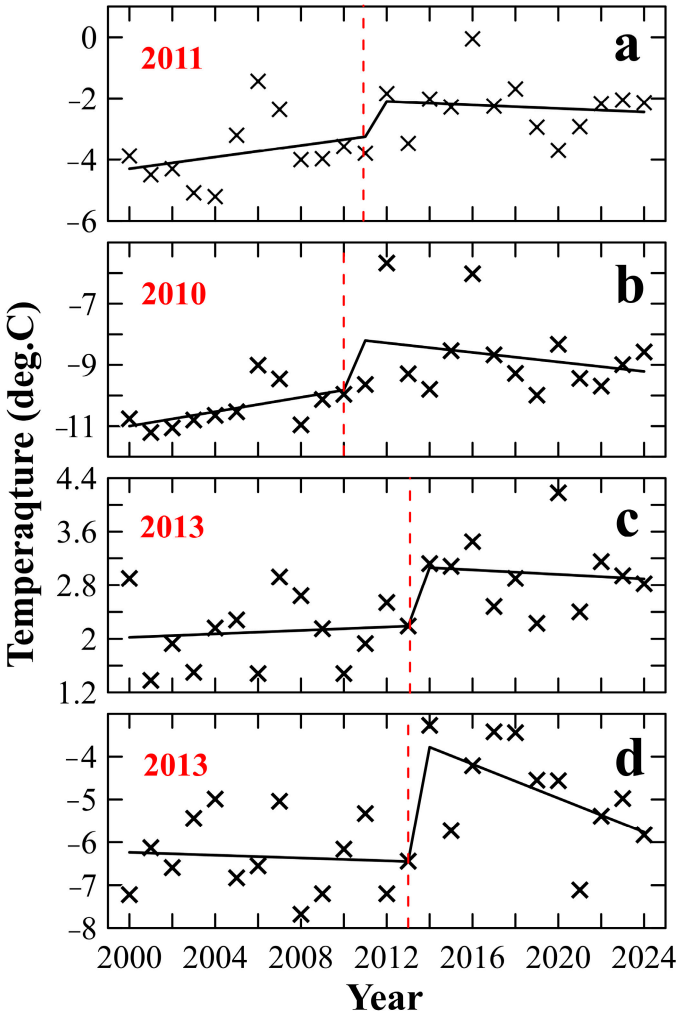

Figure 2. Statistically significant regime shifts in annual mean Arctic surface air temperatures for the period 2000–2024 at four locations: (**a**) Svalbard Airport (Svalbard, Norway), (**b**) Heiss Island (Franz Josef Land, Russia), (**c**) Zhizhgin Mayak (Arkhangelsk Oblast, Russia), (**d**) Anadyr (Chukotka, Russia). Black lines indicate linear trends derived from two-phase linear regression analysis. Dashed red lines denote years with statistically significant regime shifts; these years are also highlighted in red. See Table 1 and Table S1 for statistical details.

Table 1 lists the regime shift parameters for annual mean SAT values: breakpoint timings, pre- and post-breakpoint trends, and associated statistics. Stations showing a shift from increase to decrease were predominantly located across the major Arctic archipelagos, including Svalbard (Norway) and the Russian archipelagos of Franz Josef Land, Novaya Zemlya, and Severnaya Zemlya. A similar pattern was observed along the coast of the White Sea (Figures 1 and 2c). Stations with a decrease followed by a stronger decrease were found at Russian and US stations near the Bering Strait (Figures 1 and 2d). A regime shift characterized by an increase followed by a weaker increase was observed along the Arctic coasts of Russia, the Novosibirsk Islands, the USA, and parts of Canada (Figure 1). In contrast, the Canadian Arctic Archipelago, the Kola Peninsula (Murmansk Oblast, Russia), and parts of Finland generally exhibited continuing increasing trends (Figures 1 and 3d; Table 1). Trends from other parts of the Arctic and Subarctic (including mainland Norway, Sweden, Greenland, Iceland, part of Chukotka (Russia), and the USA) were not statistically significant. This pattern is exemplified by Thule (Greenland) in Figure 3c.

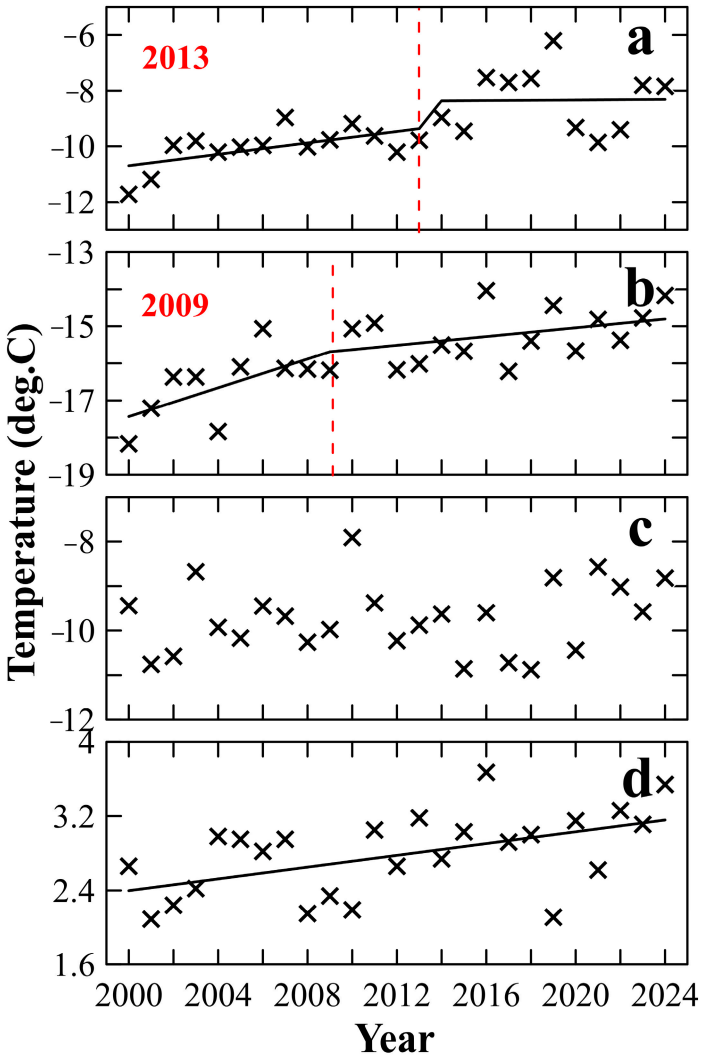

Figure 3. Same as Figure 2, but for (**a**) Barrow (Alaska, USA), (**b**) Alert (Canada), (**c**) Thule (Greenland, Denmark), and (**d**) Slettnes Fyr (Norway).

For the primary studied period (2000–2024), we applied a combination of parametric and nonparametric methods (ordinary regression, segmented regression, the Mann–Kendall test, Sen's slope estimator, the Pettitt test, and the permutation-based Buishand test) to ensure robust results even with relatively short time series. To further strengthen the reliability of our findings, we extended the analysis to the preceding 25-year interval (1975–1999). From this extended dataset, we excluded five stations with incomplete measurements across the entire period: Okunev Nos, Antipajuta, Barrow, Nuiqsut, Nome Muni. For the remaining stations, the Pettitt test detected no statistically significant breakpoints at the $p < 0.05$ level, with the sole exception of Inuvik station (Canada), where a breakpoint was identified in 1986. Given the absence of breakpoints across almost all stations in the extended period (1975–1999), and that the original (2000–2024) results were derived from a robust multi-method framework, we have high confidence in the reliability of our primary findings. These results increase the reliability of identification of change points within the 2000–2024 interval.

4. Discussion

To evaluate climatic changes in the Arctic, we analyzed annual mean surface air temperature (SAT) trends at sites located on or above the Arctic Circle from 2000 to 2024. This period captures the recent phase of Arctic climate change following the pronounced

warming of the 1990s and early 2000s [29–37], and includes the post-2012 period when some regions (e.g., the Barents and Kara Seas) exhibited a stabilization or even a partial recovery of sea ice cover despite the long-term decline [31]. Moreover, the interval is short enough to focus on contemporary processes, including possible regime shifts in temperature trends. Some studies have indicated multidecadal cyclicity in Arctic sea ice fluctuations [30–32]. Therefore, the recent reduction in ice cover observed in the Russian Arctic may cease in the coming decades [30,31].

The combination of the Mann–Kendall (MK) test and the Sen's slope estimator (SSE) revealed that only 31% of the 158 Arctic stations display a statistically significant warming trend in SAT ($p < 0.05$), while 42% show no statistically significant temperature trend over 2000–2024. Stations without any trend are located primarily along the path of warm Atlantic waters, in the coastal areas of Iceland, Greenland and mainland Norway (Figure 1). In northern Finland, stations are approximately equally divided between those showing an increasing trend and those with no significant trend. In contrast, stations on the coastal region of the Barents Sea (Kola Peninsula, Russia) show a significant warming trend (Figure 1).

Beyond linear trends, we applied the Pettitt and Buishand nonparametric tests to detect breakpoints or regime shifts. Both tests identified breakpoints at 38 stations within the 2009–2014 interval (Table 1). Among these, 36 stations demonstrate a weakening of the warming trend after the breakpoint. Notably, almost all of these stations are located in Arctic coastal areas connected to the points of inflow and spreading of warm Atlantic and Pacific waters (Figure 1). One group of stations lies on the main Arctic archipelagos: Norwegian Svalbard and the Russian archipelagos of Franz Josef Land, Severnaya Zemlya, and Novaya Zemlya. All these stations show a strong change in the temperature regime—from an increasing to a decreasing trend (Figure 1 and Table 1).

The temperature and salinity patterns of the Arctic Ocean are governed by several main processes: inflow of warm Atlantic waters through two branches (the Fram Strait and the Barents Sea branch), inflow of warm Pacific waters through the Bering Strait, river runoff, air–sea interaction, and solar heating of sea surface [29,31,32]. Atlantic water entering the Barents Sea undergoes cooling, mainly due to heat loss to the atmosphere, and subsequently spreads eastward along the eastern flank of the St. Anna trough in the Northern Kara Sea [33]. The northward-flowing Atlantic water keeps the Barents and Greenland Seas ice-free during winter [33]. Thus, the Barents Sea serves as a natural boundary between two climatic regions: the cold, stratified, seasonally ice-covered Arctic region and the warm, well-mixed, ice-free Atlantic region [33].

The North Atlantic current (which continues as the warm Atlantic water mass) plays a key role in the climate of the western Russian Arctic; however, its influence exhibits a clearly defined spatial limit [31,33,37]. By the time it reaches the Kara Sea, it has already been significantly transformed, so the Laptev and East Siberian Seas experience practically no direct impact from it [30,31,33,37]. The warmer waters of the Barents Sea (essentially transformed Atlantic waters) enter the Kara Sea through the Kara Gate Strait and the St. Anna Trough [30,37]. This influx of heat moderates the climate of the southwestern Kara Sea to some extent; whereas, for the Laptev and East Siberian seas, this moderating effect is considerably weaker [31,33,37]. The thermal regime in these seas is substantially influenced by runoff from the great Siberian rivers (Ob, Yenisei, and Lena), as well as by atmospheric circulation and the associated wind patterns [33,37]. Based on hydrological and hydrochemical data collected aboard the Russian vessel *Nikolay Kolomeytsev* in 2000, the East Siberian Sea can be divided into two zones: a western zone strongly affected by Lena River runoff, and an eastern zone under the direct influence of Pacific-derived waters [38].

Turning to our results, all stations located in the coastal zone and adjacent areas of the Kara and Laptev Seas exhibit a weakening of the annual mean SAT warming trend (i.e., an initial increase followed by a weaker increase after the breakpoint; Figure 1). The only exception is Tiksi (Buor-Khaya Bay, Laptev Sea), where SAT shows a significant warming trend ($p < 0.01$; Figure 1 and Table S1). All stations in the coastal areas of the eastern zone of the East Siberian Sea show no significant trend (Figure 1).

An interesting finding concerns SAT trends at several stations located in the coastal zone of the White Sea (an inland sea of Russia). Three of these stations (including Zhizhgin Mayak, Figure 2c and Table 1) exhibit a regime shift: SAT initially increases but then declines after the breakpoint. One station (Pjalica, Figure 1 and Table 1), situated on the opposite side of the White Sea on the Tersk coast of the Kola Peninsula, shows a weakening of the increasing temperature trend after the breakpoint. In contrast, two stations in the coastal area of the Kola Peninsula (Kandalaksha Bay of the White Sea) display a significant ($p < 0.05$) increasing temperature trend without any breakpoint (Figure 1 and Table S1). A third station with a similar increasing trend is located at Cape Kanin Nos, which serves as watershed between the Barents and White Seas.

The key difference between the White and Barents Seas is that the latter receives a substantial influx of warm Atlantic water via the Gulf Stream, keeping it ice-free year-round [30,32,33]. Some of the warm water from the Barents Sea flows through the Voronka and Gorlo Straits, but water exchange is severely restricted by bottom topography and hydrological conditions, which act as a natural barrier [39,40]. Consequently, despite its more southerly latitude, the White Sea cools rapidly and freezes over every winter [40]. Thus, the influence of warm Barents Sea waters on the White Sea and its coast is significant, but not decisive, and it is highly heterogeneous [40]. At the same time, we cannot rule out the possibility that the observed change in the SAT regime along most of the White Sea coast (i.e., weakening of the warming trend or reversal to a cooling trend) may be partly caused by a slowdown of the AMOC.

Another group of stations with a strong change in the SAT regime is located in coastal areas near the Bering Strait (on both, the Russian and U.S. sides) and along the coast of the Bering Sea in Chukotka, Russia—a region that receives inflow of warm Pacific water (Figure 1). At these stations, cooling intensifies after the breakpoint, meaning that the temperature decrease becomes steeper following the change point (Figure 1). The water masses entering the Chukchi Sea through the Bering Strait—primarily via the Alaskan Coastal Current—are warmer than the local Arctic waters [34,35,37]. After flowing into the Chukchi Sea basin, these water masses release their heat, thereby increasing both the sea surface temperature and SAT in the surrounding areas [34,35]. However, the effect of warm Bering and Chukchi waters on the Beaufort Sea is complex and not always direct [41]. For instance, increased easterly winds can hinder the transform of warm waters from the Alaskan Coastal Current into the western part of the Beaufort Sea [41].

Our results show that three stations located on the U.S. coast of the Chukchi Sea (including Kotzebue) exhibit no trend in SAT changes, whereas one station (Barrow, Figure 3a) demonstrates a pattern of a weakening warming trend after the breakpoint (Figure 1 and Table 1). It should be noted that, although the advection of warm Pacific waters into the Chukchi Sea plays an important role, coastal temperatures are largely determined by changes in atmospheric circulation, wind patterns, and solar heating [29,34,35].

The stations that exhibit the post-2009 cooling shift are located near the main gateways for warm Atlantic and Pacific water inflow to the Arctic. In these coastal zones, SAT is strongly coupled to local ocean heat transport and sea surface conditions, especially during the ice-free seasons [31–33,35]. Hence, SAT can serve as a reasonable indirect indicator of oceanic heat advection changes. A combined analysis with direct sea surface temperature

(SST) and sea surface salinity (SSS) data would strengthen the results. However, given the data constraints, SAT provides a valuable, continuous, and accessible record that captures the timing and spatial pattern of the recent regime shift.

All these findings may indicate a slowing, if not a collapse, of the AMOC and of Pacific water inflow into the Arctic Ocean. Recent modelling studies provide context for our investigations, as they highlight the critical role of the AMOC in Arctic climate [11,12,42]. Simulations have shown that a weakened AMOC would slow the decline in Arctic sea ice [42], and that a collapse of the AMOC could even lead to a rapid expansion of sea ice [11,12]. Such a tipping event would cool Europe by several degrees and bring about Little Ice Age-type conditions, possibly as early as the 21st century [11,12]. Some recent simulations indicate the imminent approach of an AMOC collapse [11,12]. Other models, however, predict only a slowing of the AMOC without its collapse in this century [42]. This weakening would also reduce SAT around northwestern Europe, increasing related hazards and coastal risks, because these regions are warmed by the North Atlantic Current [43]. Moreover, recent research has established a clear decadal relationship between Arctic surface air temperature and AMOC changes [44]. The authors demonstrate that AMOC and Arctic SAT vary in phase on decadal timescales [44]. This established relationship supports our interpretation that the temperature regime shifts we detected may reflect underlying changes in ocean circulation patterns.

Our study does not claim to detect a complete AMOC collapse. Rather, it identifies a potential early signal of changing ocean circulation patterns based on statistically significant breakpoints in Arctic temperature records. Given the complex interplay of multiple forcing factors in the Arctic, including atmospheric circulation modes (such as NAO/AO), wind patterns, air–sea–ice exchange, local land–ocean interactions, and solar heating, our analysis cannot definitively attribute the observed breakpoints solely to AMOC changes. However, the combination of statistically robust breakpoints and their geographic clustering near major ocean inflow pathways makes our interpretation a plausible and testable hypothesis. We propose that these temperature regime shifts may represent early manifestations of changing ocean circulation patterns, including contributions from both the Atlantic and Pacific, even if the full tipping transition remains decades away.

Regardless of the underlying cause, our results are useful for assessing Arctic navigation potential, natural resource extraction on shelves and in coastal regions, and the development of economic and trade opportunities in the Arctic coastal zone and adjacent areas.

5. Conclusions

This study aimed to assess whether a slowdown, or even collapse of the AMOC, is likely in the near future. For this purpose, we analyzed SAT trends over recent decades at sites located in coastal regions of the Arctic Ocean and adjacent areas. Between 2000 and 2024, only 38% of Arctic stations showed statistically significant SAT warming, while 35% of stations exhibited no trend. Stations without trends clustered along the path of warm Atlantic waters (Iceland, Greenland, mainland Norway) and in parts of Fennoscandia.

Abrupt changes in SAT were detected at 24% of stations, with breakpoints concentrated between 2009 and 2014. The dominant pattern (36 of 38 stations) is a weakening of the previous warming trend, including reversals from warming to cooling in key Arctic archipelagos (Svalbard, Franz Josef Land, Severnaya Zemlya, Novaya Zemlya).

The observed regime shifts are spatially coherent with regions influenced by Atlantic water inflow (Barents Sea, Kara Sea, White Sea) and Pacific water inflow (Bering Strait, Bering and Chukchi Seas). This suggests a possible causal link to changes in poleward heat transport, particularly AMOC strength.

The pattern of cooling or slowed warming in coastal areas directly warmed by Atlantic and Pacific currents is consisted with modelled predictions of an AMOC slowdown or collapse. Although alternative drivers (e.g., atmospheric circulation, solar activity, river runoff) cannot be ruled out, the timing and spatial distribution of the observed changes support the hypothesis that an AMOC weakening may already be affecting Arctic SAT, posing potential risks to natural systems and human societies.

If AMOC continues to weaken or collapses, Arctic warming could decelerate or reverse in certain regions, potentially slowing sea ice decline, reducing navigation windows along the Northern Sea Route, and altering the feasibility of coastal resource extraction. These possibilities need to be taken into account in long-term economic and infrastructure planning.

Supplementary Materials: The following supporting information can be downloaded at: https://www.mdpi.com/article/10.3390/geosciences16060239/s1, Table S1: Station coordinates and temperature trends (2000–2004).

Author Contributions: Conceptualization, E.A.K. and O.I.S.; methodology, E.A.K. and O.I.S.; software, E.A.K.; validation, E.A.K., O.I.S. and D.V.M.; formal analysis, E.A.K., O.I.S. and D.V.M.; investigation, E.A.K.; resources, O.I.S. and D.V.M.; data curation, E.A.K.; writing—original draft preparation, E.A.K.; writing—review and editing, E.A.K., O.I.S. and D.V.M.; visualization, E.A.K. and O.I.S.; supervision, E.A.K., O.I.S. and D.V.M.; project administration, D.V.M.; funding acquisition, D.V.M. All authors have read and agreed to the published version of the manuscript.

Funding: This research was carried out within the framework of the State Task of the Institute of North Industrial Ecology Problems, Kola Science Centre RAS (project No. FMEZ-2025-0044).

Data Availability Statement: Meteorological data are contained within the article, and all data sources are mentioned.

Acknowledgments: The authors are grateful to Vladimir I. Lagovsky for their valuable discussions. The authors would like to thank the editor and anonymous reviewers for their insightful comments and constructive suggestions, which significantly improved the quality of this paper.

Conflicts of Interest: The authors declare no conflicts of interest.

Abbreviations

The following abbreviations are used in this manuscript:

AMOC	Atlantic Meridional Overturning Circulation
IPCC	Intergovernmental Panel on Climate Change
SAT	Surface air temperature
GSM	Grand Solar Minimum

References

1. IPCC. Summary for Policymakers. In *Climate Change 2023: Synthesis Report. Contribution of Working Groups I, II and III to the Sixth Assessment Report of the Intergovernmental Panel on Climate Change*; Core Writing Team, Lee, H., Romero, J., Eds.; IPCC: Geneva, Switzerland, 2023; pp. 1–34. [CrossRef]
2. Zhang, Y.; Sun, X.; Zha, Y.; Wang, K.; Chen, C. Changing Arctic Northern Sea Route and Transpolar Sea Route: A prediction of route changes and navigation potential before Mid-21st century. *J. Mar. Sci. Eng.* **2023**, *11*, 2340. [CrossRef]
3. Sharapov, D. Northern Sea Route and climate change. *E3S Web Conf.* **2023**, *460*, 09019. [CrossRef]
4. Krivorotov, A.; Finger, M. State-owned enterprises in the Arctic. In *The GlobalArctic Handbook*; Finger, A., Heininen, L., Eds.; Springer: Cham, Switzerland, 2019; pp. 45–62. [CrossRef]
5. Krivovichev, S. Editorial for Special Issue "Arctic Mineral Resources: Science and Technology". *Minerals* **2019**, *9*, 192. [CrossRef]
6. Moe, A. A new Russian policy for the Northern Sea Route? State interests, key stakeholders and economic opportunities in changing times. *Polar J.* **2020**, *10*, 209–227. [CrossRef]

7. Wang, S.; Yu, F.; Min, C.; He, Y.; Pan, R.; Shu, Q. Projected navigability of Arctic shipping routes based on climate model FIO-ESM v2.1. *Anthropocene* **2024**, *47*, 100445. [CrossRef]
8. Lamazhapov, E. Friends in need? Russo-Chinese cooperation in the Arctic. In *Handbook of the Politics of the Arctic*, 2nd ed.; Hønneland, G., Østhagen, A., Rottem, S.V., Eds.; Edward Elgar Publishing: Cheltenham, UK, 2026; pp. 451–468. [CrossRef]
9. Srokosz, M.A.; Bryden, H.L. Observing the Atlantic meridional overturning circulation yields a decade of inevitable surprises. *Science* **2015**, *348*, 1255575. [CrossRef] [PubMed]
10. Weijer, W.; Cheng, W.; Garuba, O.A.; Hu, A.; Nadiga, B.T. CMIP6 models predict significant 21st century decline of the Atlantic meridional overturning circulation. *Geophys. Res. Lett.* **2020**, *47*, e2019GL08607. [CrossRef]
11. van Westen, R.M.; Baatsen, M.L.J. European temperature extremes under different AMOC scenarios in the Community Earth System Model. *Geophys. Res. Lett.* **2025**, *52*, e2025GL114611. [CrossRef]
12. Dijkstra, H.A.; van Westen, R.M. The probability of an AMOC collapse onset in the twenty-first century. *Annu. Rev. Mar. Sci.* **2026**, *18*, 23–46. [CrossRef] [PubMed]
13. Li, H.; Fedorov, A.V. Persistent freshening of the Arctic Ocean and changes in the North Atlantic salinity caused by Arctic sea ice decline. *Clim. Dyn.* **2022**, *57*, 2995–3013. [CrossRef]
14. Mörner, N.-A. The approaching new Grand Solar Minimum and Little Ice Age climatic conditions. *Nat. Sci.* **2015**, *7*, 510–518. [CrossRef]
15. Soon, W. Solar Arctic-mediated climate variation on multidecadal to centennial timescales: Empirical evidence, mechanistic explanation, and testable consequences. *Phys. Geogr.* **2009**, *30*, 144–184. [CrossRef]
16. Lean, J.R.; Beer, J.; Bradley, R. Reconstruction of solar irradiance since 1610, Implications for climate change. *Geophys. Res. Lett.* **1995**, *22*, 3195–3198. [CrossRef]
17. Lockwood, M.; Harrison, R.G.; Woolings, T.; Solanki, S.K. Are cold winters in Europe associated with low solar activity? *Environ. Res. Lett.* **2010**, *5*, 024001. [CrossRef]
18. Abdussamatov, H.I. The new Little Ice Age has started. In *Evidence-Based Climate Science*, 2nd ed.; Easterbrook, D.J., Ed.; Elsevier: Amsterdam, The Netherlands, 2016; pp. 307–328. [CrossRef]
19. Zharkova, V. Modern Grand Solar Minimum will lead to terrestrial cooling. *Temperature* **2020**, *7*, 217–222. [CrossRef] [PubMed]
20. Ineson, S.; Maycock, A.C.; Gray, L.J.; Scaife, A.A.; Dunstone, N.J.; Harder, J.W.; Knight, J.R.; Lockwood, M.; Manners, J.C.; Wood, R.A. Regional climate impacts of a possible future grand solar minimum. *Nat. Commun.* **2015**, *6*, 7535. [CrossRef] [PubMed]
21. Kasatkina, E.A.; Shumilov, O.I.; Timonen, M. Neural network-based climate prediction for the 21st century using the Finnish multi-millennial tree-ring chronology. *Geosciences* **2024**, *14*, 212. [CrossRef]
22. GISTEMP Team. *GISS Surface Temperature Analysis (GISTEMP), Version 4*; NASA Goddard Institute for Space Studies: New York, NY, USA, 2024. Available online: https://data.giss.nasa.gov/gistemp (accessed on 20 December 2025).
23. Kendall, M.G. *Rank Correlation Methods*, 4th ed.; Griffin: London, UK, 1970.
24. Liu, L.; Xu, Z.-X.; Huang, J.-H. Spatio-temporal variation and abrupt changes for major climate variables in the Taihu Basin, China. *Stoch. Environ. Res. Risk Assess.* **2012**, *26*, 777–791. [CrossRef]
25. Sen, P.K. Estimates of the regression coefficient based on Kendall's tau. *J. Am. Stat. Assoc.* **1968**, *63*, 1379–1389. [CrossRef]
26. Pettitt, A. A non-parametric approach to the change-point problem. *J. R. Stat. Soc. Ser. C-Appl.* **1979**, *28*, 126–135. [CrossRef] [PubMed]
27. Buishand, T.A. Tests for detecting a shift in the mean of hydrological time series. *J. Hydrol.* **1984**, *73*, 51–69. [CrossRef]
28. Kabbilawsh, P.; Kumar, D.S.; Chithra, N.R. Assessment of temporal homogeneity of long-term rainfall time-series datasets by applying classical homogeneity tests. *Environ. Dev. Sustain.* **2024**, *26*, 16757–16801. [CrossRef]
29. Perovich, D.K.; Light, B.; Eicken, H.; Jones, K.F.; Runciman, K. Increasing solar heating of the Arctic Ocean and adjacent seas, 1979–2005: Attribution and role in the ice-albedo feedback. *Geophys. Res. Lett.* **2007**, *34*, L19505. [CrossRef]
30. Matishov, G.; Moiseev, D.; Lyubina, O.; Zhichkin, A.; Dzhenyuk, S.; Karamushko, O.; Frolova, E. Climate and cyclic hydrobiological changes of the Barents Sea from the twenty-first centuries. *Polar Biol.* **2012**, *35*, 1773–1790. [CrossRef]
31. Matishov, G.G.; Dzhenyuk, S.L.; Moiseev, D.V.; Zhichkin, A.P. Pronounced anomalies of air, water, ice conditions in the Barents and Kara Seas, and the Sea of Azov. *Oceanologia* **2014**, *56*, 445–460. [CrossRef]
32. Levitus, S.; Matishov, G.; Seidov, D.; Smolyar, I. Barents Sea multidecadal variability. *Geophys. Res. Lett.* **2009**, *36*, L19604. [CrossRef]
33. Smedsrud, L.H.; Esau, I.; Ingvaldsen, R.B.; Eldevik, T.; Haugan, P.M.; Li, C.; Lien, V.S.; Olsen, A.; Omar, A.M.; Otterå, O.H.; et al. The role of the Barents Sea in the Arctic climate system. *Rev. Geophys.* **2013**, *51*, 415–449. [CrossRef]
34. Wood, K.R.; Bond, N.A.; Danielson, S.L.; Overland, J.E.; Salo, S.A.; Stabeno, P.J.; Whitefield, J. A decade of environmental change in the Pacific Arctic region. *Prog. Oceanogr.* **2015**, *136*, 12–31. [CrossRef]
35. Rostov, I.D.; Dmitrieva, E.V.; Vorontsov, A.A. Climatic changes in thermal conditions of sea areas in the Eastern Arctic at the turn of the 20th and 21st centuries. *Russ. Meteorol. Hydrol.* **2019**, *7*, 440–451. [CrossRef]

36. Polyakov, I.V.; Pnyushkov, A.V.; Charette, M.; Cho, K.-H.; Jung, J.; Kipp, L.; Muilwijk, M.; Whitmore, L.; Yang, E.J.; Yoo, J. Atlantification advances into the Amerasian Basin of the Arctic Ocean. *Sci. Adv.* **2025**, *11*, eadq7580. [CrossRef] [PubMed]
37. Rudels, B.; Jones, E.P.; Schauer, U.; Eriksson, P. Atlantic sources of the Arctic Ocean surface and halocline waters. *Pol. Res.* **2004**, *23*, 181–208. [CrossRef]
38. Semiletov, I.; Dudarev, O.; Luchin, V.; Charkin, A.; Shin, K.-H.; Tanaka, N. The East Siberian Sea as a transition zone between Pacific-derived waters and Arctic shelf waters. *Geophys. Res. Lett.* **2005**, *32*, L10614. [CrossRef]
39. Berger, V.Y.; Naumov, A.D. General features of the White Sea. In *Scientific Cooperation in the Russian Arctic: Ecology of the White Sea with Emphasis on its Deep Basin*; Rachor, E., Ed.; Alfred Wegener Institut für Polar und Meeresforschung: Bremerhaven, Germany, 2000; pp. 3–9. [CrossRef]
40. Filatov, N.N.; Pozdnyakov, D.V.; Ingebeikin, J.I.; Zdorovenov, R.E.; Melentyev, V.V.; Tolstikov, A.V.; Pettersson, L.H. Oceanographic regime. In *White Sea: Its Marine Environment and Ecosystem Dynamics Influenced by Global Change*; Filatov, N., Pozdnyakov, D., Johannssen, O.M., Pettersson, L.H., Bobylev, L.P., Eds.; Springer: Berlin/Heidelberg, Germany, 2005; pp. 73–154. [CrossRef]
41. Okkonen, S.R.; Ashjian, C.J.; Campbell, R.G.; Maslowski, W.; Clement-Kinney, J.L.; Potter, R. Intrusion of warm Bering/Chukchi waters onto the shelf in the western Beaufort Sea. *J. Geophys. Res.* **2009**, *114*, C00A11. [CrossRef]
42. Baker, J.A.; Bell, M.J.; Jackson, L.C.; Vallis, G.K.; Watson, A.J.; Wood, R.A. Continued Atlantic overturning circulation even under climate extremes. *Nature* **2025**, *638*, 987–994. [CrossRef] [PubMed]
43. Kim, S.-K.; Kim, H.-J.; Dijkstra, H.A.; An, S.-I. Slow and soft passage through tipping point of the Atlantic Meridional Overturning Circulation in a changing climate. *npj Clim. Atmos. Sci.* **2022**, *5*, 13. [CrossRef]
44. Zhao, B.; Lin, P.; Liu, H.; Hu, A.; Chen, X.; Yang, L. Decadal relationship between Arctic SAT and AMOC changes modulated by the North Pacific Oscillation. *J. Geophys. Res. Atmos.* **2024**, *129*, e2024JD041577. [CrossRef]

Disclaimer/Publisher's Note: The statements, opinions and data contained in all publications are solely those of the individual author(s) and contributor(s) and not of MDPI and/or the editor(s). MDPI and/or the editor(s) disclaim responsibility for any injury to people or property resulting from any ideas, methods, instructions or products referred to in the content.